DNA-PK Promotes DNA End Resection at DNA Double Strand Breaks in G_0 cells

Faith C. Fowler[1,2], Bo-Ruei Chen[3], Nicholas Zolnerowich[4], Wei Wu[4], Raphael Pavani[4], Jacob Paiano[4], Chelsea Peart[2], André Nussenzweig[4], Barry P. Sleckman[3*], and Jessica K. Tyler[2*]

[1]Weill Cornell Medicine Pharmacology Graduate Program, New York, NY 10065, USA

[2] Weill Cornell Medicine, Department of Pathology and Laboratory Medicine, New York, NY 10065, USA

[3] Department of Medicine, Division of Hematology and Oncology, O'Neal Comprehensive Cancer Center, University of Alabama at Birmingham, Birmingham, AL, 35294, USA.

[4]Laboratory of Genome Integrity, National Cancer Institute, Bethesda, MD, 20892

*Corresponding Authors: jet2021@med.cornell.edu and bps@uab.edu

Abstract

DNA double-strand break (DSB) repair by homologous recombination is confined to the S and G_2 phases of the cell cycle partly due to 53BP1 antagonizing DNA end resection in G_1 phase and non-cycling quiescent (G_0) cells where DSBs are predominately repaired by non-homologous end joining (NHEJ). Unexpectedly, we uncovered extensive MRE11- and CtIP-dependent DNA end resection at DSBs in G_0 mammalian cells. A whole genome CRISPR/Cas9 screen revealed the DNA-dependent kinase (DNA-PK) complex as a key factor in promoting DNA end resection in G_0 cells. In agreement, depletion of FBXL12, which promotes ubiquitylation and removal of the KU70/KU80 subunits of DNA-PK from DSBs, promotes even more extensive resection in G_0 cells. In contrast, a requirement for DNA-PK in promoting DNA end resection in proliferating cells at the G_1 or G_2 phase of the cell cycle was not observed. Our findings establish that DNA-PK uniquely promotes DNA end resection in G_0, but not in G_1 or G_2 phase cells, and has important implications for DNA DSB repair in quiescent cells.

Introduction

DNA double-strand breaks (DSBs) are particularly deleterious lesions which, if left unrepaired, can lead to cell death, or if repaired aberrantly, can lead to oncogenic chromosomal translocations and deletions (Jackson and Bartek 2009). Eukaryotic cells utilize two main mechanisms of DSB repair: non-homologous end joining (NHEJ), where the broken DNA ends are ligated together with minimal processing of the DNA termini; and homologous recombination (HR), which uses a homologous sequence, usually on a sister chromatid, as a template for accurate DNA repair. Because HR relies on a homologous template for accurate repair, HR is mostly restricted to S and G_2 phases of

the cell cycle when sister chromatids exist. On the other hand, cells can employ NHEJ in any phase of the cell cycle and it is the only option in quiescent (G_0) cells and G_1 phase cells (Scully et al. 2019).

Extensive DNA end resection of the broken DNA ends, which generates long tracts of 3' ssDNA overhangs at DSBs, is a critical step in committing the cell to use HR to repair DSBs. DNA end resection is initiated by nucleases MRE11 and CtIP, and subsequently extended by nucleases including EXO1 and DNA2/BLM (Paull and Gellert 1998; Trujillo et al. 1998; Sartori et al. 2007; Gravel et al. 2008; Mimitou and Symington 2008; Zhu et al. 2008; Bunting et al. 2010). The 3' ssDNA overhangs are quickly bound by the single-stranded binding protein trimer replication protein A (RPA) to stabilize and protect the ssDNA, and later in repair RPA is replaced by the RAD51 recombinase protein that leads to the homology search to find a homologous template to achieve accurate HR repair (Sugiyama and Kowalczykowski 2002; San Filippo et al. 2008; Wright et al. 2018). NHEJ is initiated by the KU70/KU80 heterodimer binding to broken DNA ends (Zahid et al. 2021). KU70/KU80 recruits the DNA-dependent protein kinase catalytic subunit (DNA-PKcs) which together form a complex called DNA-PK (Gottlieb and Jackson 1993; Hammarsten and Chu 1998). Once the DNA-PK complex is formed, the KU heterodimer translocates inwards along the DNA and DNA-PKcs remains at the DNA ends, undergoing activation via conformational changes mediated by autophosphorylation of the ABCDE cluster (Yaneva et al. 1997; Chen et al. 2021b). Recent cryo-EM structures of DNA-PK also implicate dimerization of DNA-PK as important in recruiting downstream NHEJ factors by bringing broken DNA ends together (Chaplin et al. 2021; Zha et al. 2021). In addition to autophosphorylation, DNA-PKcs phosphorylates members of the NHEJ

machinery, including the KU heterodimer, XRCC4, XLF, and Artemis (Bartlett and Lees-Miller 2018).

The critical bifurcation point in the choice to use HR or NHEJ to repair DSBs is the processing of broken DNA ends to form single-stranded 3' DNA overhangs, which blocks NHEJ and commits the cell to HR (Symington and Gautier 2011). Therefore, DNA end resection is tightly regulated to prevent aberrant DNA end resection in G_0 and G_1 phase cells, where NHEJ is the major DSB repair pathway. Several factors have been identified as critical DNA end protection factors that limit resection of DNA DSBs including 53BP1, RIF1, and the Shieldin complex. The proposed mechanism of action of 53BP1 and its downstream effectors include acting as a physical barrier to protect DNA ends from nucleases and promoting DNA polymerase α activity to quickly fill in any resected ends (Dev et al. 2018; Mirman et al. 2018; Noordermeer et al. 2018; Setiaputra and Durocher 2019; Paiano et al. 2021). Additionally, KU70/KU80 has also been shown in budding yeast *Saccharomyces cerevisiae* to inhibit DNA end resection in G_1 and G_2 phases of the cell cycle, and in S phase in mammalian cells (Lee et al. 1998; Clerici et al. 2008; Shao et al. 2012).

While nuclease activity is largely limited in G_0/G_1 phase cells to prevent aberrant DNA end resection, evidence exists suggesting that nuclease-mediated DNA end processing occurs at some DSBs in G_0/G_1. For example, Artemis is required to open hairpin-sealed DNA ends generated during V(D)J recombination in lymphocytes (Menon and Povirk 2016). Additionally, DNA end resection has been observed in G_1 phase after DNA damage at complex DNA lesions (Averbeck et al. 2014; Biehs et al. 2017), suggesting that DNA end resection is not completely inhibited in the absence of sister

87 chromatids. To investigate what additional factors may regulate DNA end resection in
88 cells lacking sister chromatids, we performed a genome-wide CRISPR/Cas9 screen for
89 genes whose inactivation either increases or decreases RPA bound to chromatin after
90 irradiation (IR) in G_0-arrested murine cells. We discovered, unexpectedly, that KU70,
91 KU80, and DNA-PKcs promote extensive DNA end resection in G_0 cells, but not in G_1 or
92 G_2 phases of the cell cycle.
93

Results

RPA associates with IR-induced DNA DSBs in G_0 cells:

Murine pre-B cells transformed with Abelson murine leukemia virus (termed abl pre-B cells hereafter) continuously proliferate *in vitro* and can be efficiently arrested in G_0, also referred to as the quiescent state, upon treatment with the abl kinase inhibitor imatinib (Figure S1A) (Bredemeyer et al. 2006; Chen et al. 2021a). To investigate how DNA end resection is regulated in G_0 cells, we used a flow cytometric approach to assay RPA bound to chromatin after detergent extraction of soluble RPA, as a proxy for ssDNA generated at DSBs after exposing cells to irradiation (IR) (Forment et al. 2012; Chen et al. 2021a). This assay was performed in abl pre-B cell lines deficient in DNA Ligase IV (*Lig4*$^{-/-}$), to maximize our ability to detect chromatin-bound RPA at DSBs, given that completion of NHEJ is prevented in the absence of DNA Ligase IV. We also performed the analysis in *Lig4*$^{-/-}$*:53bp1*$^{-/-}$ abl pre-B cells which lack the DNA end protection protein 53BP1 and accumulate high levels of RPA on chromatin after IR (Chen et al. 2021a). In agreement with our previous work, we detected a high level of chromatin-bound RPA in G_0-arrested *Lig4*$^{-/-}$*:53bp1*$^{-/-}$ abl pre-B cells after IR, consistent with the role of 53BP1 in DNA end protection (Figure 1A). Surprisingly, we also observed RPA associated with chromatin after IR of G_0-arrested *Lig4*$^{-/-}$ abl pre-B cells, although at lower levels than in *Lig4*$^{-/-}$*:53bp1*$^{-/-}$ abl pre-B cells (Figure 1A). Moreover, the increase in IR-induced chromatin-bound RPA does not require DNA Ligase IV deficiency as we were able to observe similar results using the RPA flow cytometric assay in wild-type (WT) abl pre-B cells arrested in G_0 (Figure S1B). These data indicate that extensive DNA end resection

116 occurs at DSBs in G_0 cells, despite the presence of the DNA end protection proteins
117 53BP1 and KU70/KU80.

118 To determine whether higher levels of chromatin-bound RPA in irradiated G_0-
119 arrested *Lig4*$^{-/-}$ abl pre-B cells is a result of DNA end resection, we depleted the nucleases
120 that are required for the initiation of DNA end resection during HR in cycling cells. We
121 found that the depletion of CtIP or MRE11 reduced the levels of RPA on chromatin in
122 irradiated G_0-arrested *Lig4*$^{-/-}$ abl pre-B cells (Figure 1B and S1C), indicating that the RPA
123 we observe with our flow cytometric assay after IR is indeed a result of DNA end
124 resection.

125 To determine whether the DNA end resection that we observed was unique to abl
126 pre-B cells or not, we performed the RPA flow cytometric chromatin association assay in
127 the human breast epithelial cell line MCF10A. We arrested the MCF10A cells in G_0 by
128 EGF deprivation (Chen et al. 2021a). Similar to *Lig4*$^{-/-}$ and WT abl pre-B cells in G_0, we
129 observed IR-induced chromatin-bound RPA in G_0 MCF10A cells (Figure S1D), consistent
130 with DNA end resection occurring in these cells at DSBs. RPA binding to ssDNA
131 surrounding DSBs often form distinct nuclear foci that can be easily detected by
132 immunofluorescence staining and microscopy analysis (Golub et al. 1998). Therefore, we
133 performed immunofluorescence staining for RPA in EGF-deprived MCF10A cells. We
134 observed discrete IR-induced RPA foci, consistent with the RPA associated with ssDNA
135 accumulating at DNA damage sites (Figure 1C). Together, these results suggest that
136 broken DNA ends are resected in a CtIP and MRE11-dependent manner, leading to RPA
137 accumulation on ssDNA in G_0 mammalian cells.
138

DNA end resection and RPA loading occurs at site-specific DSBs in G_0 cells:

As irradiation induces DNA base lesions and single-stranded DNA breaks in addition to DSBs, it could potentially complicate our analysis of DNA end processing at regions surrounding DSBs. Therefore, we investigated DSBs at specific locations in the mouse genome upon induction of the *AsiSI* endonuclease. We performed RPA chromatin immunoprecipitation sequencing (RPA ChIP-seq) after induction of *AsiSI* DSBs in G_0-arrested *Lig4*$^{-/-}$ abl pre-B cells. We detected RPA binding adjacent to *AsiSI* DSBs, consistent with ssDNA generated by resection around DNA DSBs (Paiano et al. 2021) (Figure 1D and S1E). Moreover, the association of RPA with chromatin was strand specific around the DSBs, consistent with the 5'-3' nature of DNA end resection which generates 3' ssDNA overhangs (Paiano et al. 2021) (Figure 1D). To determine the extent of DNA end processing in G_0 cells, we performed END-seq (Canela et al. 2016; Wong et al. 2021) to directly measure DNA end resection at nucleotide resolution at *AsiSI*-induced DSBs. Using END-seq, we detected extensive DNA end resection in G_0-arrested *Lig4*$^{-/-}$ abl pre-B cells at 4 and 8 hours after *AsiSI* DSB induction (Figure 1E). Together, these data indicate that in G_0-arrested cells, DNA ends are resected at DSBs induced by IR or site-specific endonucleases, generating ssDNA that is bound by RPA.

A CRISPR/Cas9 screen identifies the DNA-PK complex as promoting DNA end resection in G_0 cells:

To identify factors that influence DNA end resection in G_0 cells, we performed a genome-wide CRISPR/Cas9 screen in G_0-arrested *Lig4*$^{-/-}$ abl pre-B cells 2 hours after irradiation to identify factors that either promote or impair DNA end resection (Figure 2A).

We isolated the 10% of cells with the lowest RPA (low RPA) and the 10% cells with the highest RPA (high RPA) staining intensity using our RPA flow cytometric assay followed by flow assisted cell sorting. We then amplified the guide RNAs (gRNAs) in these populations of cells and determined their frequencies using high throughput sequencing. gRNAs enriched in the low RPA staining population correspond to genes encoding proteins that normally promote DNA end resection, while gRNAs enriched in the high RPA population correspond to genes encoding proteins that normally impair resection. In this screen we identified several gRNAs enriched in the low RPA staining population to *Rbbp8* which encodes the nuclease CtIP, and *Nbn,* which encodes the NBN subunit of the MRE11-RAD50-NBN (MRN) complex, consistent with their established roles in promoting DNA end resection (Figure 2B). Unexpectedly, we also found gRNAs of *Ku70*, *Ku80*, and *Prkdc* (the gene encoding DNA-PKcs) highly enriched in our low RPA population (Figure 2B). This suggested that DNA-PK may promote DNA end resection in G_0 cells, contrary to the established role of these factors in preventing DNA end resection in other phases of the cell cycle.

To validate the screen and determine if DNA-PK is required for DNA end resection, we generated *Lig4*$^{-/-}$*:Prkdc*$^{-/-}$ abl pre-B cells that do not express DNA-PKcs by CRISPR/Cas9-mediated gene inactivation (Figure S2A). G_0-arrested *Lig4*$^{-/-}$*:Prkdc*$^{-/-}$ abl pre-B cells had lower levels of chromatin-bound RPA after IR compared to *Lig4*$^{-/-}$ abl pre-B cells (Figure 2C). DNA-PKcs and Ataxia-telangiectasia mutated (ATM) are two major serine/threonine kinases that are activated in response to DNA DSBs and share some overlapping functions due to similar substrate specificity (Blackford and Jackson 2017). Because DNA-PKcs but not ATM was identified in our screen, we wanted to determine if

the pro-resection activity in G_0-arrested cells is unique to DNA-PKcs or also shared by ATM. We treated G_0-arrested *Lig4*$^{-/-}$ abl pre-B cells with the ATM inhibitor KU55933 or the DNA-PKcs inhibitor NU7441 before IR and performed flow cytometric analysis of IR-induced chromatin-bound RPA. In contrast to the consistent reduction in the levels of chromatin-bound RPA observed in G_0-arrested *Lig4*$^{-/-}$ abl pre-B cells treated with DNA-PKcs inhibitor, ATM inhibition did not have a detectable effect on the levels of IR-induced binding of RPA in G_0-arrested *Lig4*$^{-/-}$ abl pre-B cells (Figure 2D and S2B). The role of DNA-PK in promoting DNA end resection in G_0 is not limited to murine abl pre-B cells as we also observed a reduced number of IR-induced RPA foci in G_0-arrested human MCF10A cells upon inhibition of DNA-PKcs (Figure S2C). These results indicate that DNA-PKcs activity, but not ATM, uniquely promotes resection and RPA binding to damaged chromatin after IR in G_0 cells.

To directly observe if DNA-PKcs influenced DNA end resection at DSBs, we performed nucleotide resolution END-seq on G_0-arrested *Lig4*$^{-/-}$ abl pre-B cells with and without DNA-PKcs inhibitor treatment before the induction of *AsiSI* DSBs. Consistent with our RPA flow cytometric assay results, DNA-PKcs inhibitor-treated G_0-arrested *Lig4-/-* abl pre-B cells showed greatly reduced END-Seq signals distal to DSBs, consistent with limited DNA end processing when DNA-PK is inactivated (Figure 2E and S2D). These results demonstrate that DNA-PK activity promotes DNA end resection of DSBs in G_0 mammalian cells.

FBXL12 inhibits KU70/KU80-dependent DNA end resection in G_0 cells:

Given that DNA-PKcs promotes DNA end resection in G_0 cells (Figure 2C, 2D, 2E), and that *Ku70* and *Ku80* were enriched in the low RPA loading population of cells in the CRISPR/Cas9 screen (Figure 2B), we determined whether KU70/KU80 may also promote resection in G_0 cells. We generated *Lig4*$^{-/-}$*:Ku70*$^{-/-}$ abl pre-B cells and measured DNA end resection using our RPA flow cytometric approach. Consistent with our observations in DNA-PK inhibitor-treated G_0-arrested *Lig4*$^{-/-}$ abl pre-B cells and *Lig4*$^{-/-}$*:Prkdc*$^{-/-}$ abl pre-B cells, the level of chromatin-bound RPA after IR was greatly reduced in G_0-arrested *Lig4*$^{-/-}$*:Ku70*$^{-/-}$ abl pre-B cells compared to *Lig4*$^{-/-}$ abl pre-B cells (Figure 3A and S3A). As such, the entire DNA-PK complex is required for DNA end resection in G_0 cells.

KU70/KU80 is removed from DSBs via ubiquitylation, which has been shown to be mediated by E3 ligases including RNF138, RNF8, RNF126, and the SCF^{Fbxl12} complex (Postow et al. 2008; Feng and Chen 2012; Postow and Funabiki 2013; Ismail et al. 2015; Ishida et al. 2017). In agreement, gRNAs of *Fbxl12*, which encodes the substrate recognition subunit FBXL12 of the SCF^{Fbxl12} E3 ubiquitin ligase complex, were highly enriched in our screen in the high RPA staining cell population (Figure 2B), consistent with the idea that the persistent presence of KU70/KU80 at DSBs in cells lacking FBXL12 would lead to persistent DNA end resection. Indeed, we observed that in G_0-arrested *Lig4*$^{-/-}$*:Fbxl12*$^{-/-}$ abl pre-B cells, the level of IR-induced chromatin-bound RPA increased compared to *Lig4*$^{-/-}$ abl pre-B cells (Figure 3B and Fig S3B). Given the role of FBXL12 on limiting the levels of KU70/KU80 at broken DNA ends, we tested whether the increased DNA end resection phenotype in *Lig4*$^{-/-}$*:Fbxl12*$^{-/-}$ abl pre-B cells depended on DNA-PK activity or the presence of the KU70/KU80 complex. Indeed, inhibition of DNA-PK with

NU7441 (Figure 3C) and depletion of KU70 (Figure 3D and Fig S3C) in G_0-arrested *Lig4*$^{-/-}$*:Fbxl12*$^{-/-}$ abl pre-B cells prevented excessive accumulation of RPA on chromatin after IR. Our results suggest that the ability of DNA-PK to promote DNA end resection in G_0 cells is regulated through maintaining proper levels of KU70/KU80 at DNA DSBs by the SCF^{Fbxl12} E3 ubiquitylation complex.

DNA-PK uniquely promotes DNA end resection exclusively in G_0 cells:

KU70/KU80 have been shown to prevent DNA end resection in G_1 and G_2 phases in budding yeast and in S phase in mammalian cells but has not been examined in G_0 cells (Lee et al. 1998; Clerici et al. 2008; Shao et al. 2012). Thus, we set out to determine whether DNA-PK-dependent DNA end resection is limited to G_0 or can occur in other phases of the cell cycle. To this end, we compared the levels of IR-induced chromatin bound RPA in *Lig4*$^{-/-}$, *Lig4*$^{-/-}$*:Prkdc*$^{-/-}$ and *Lig4*$^{-/-}$*:Ku70*$^{-/-}$ abl pre-B cells arrested in G_0 by imatinib, arrested in G_2 by the CDK1 inhibitor RO3306, and in G_1 phase (cells with 2N DNA) in a proliferating population. In contrast to G_0 cells, loss of DNA-PKcs (*Lig4*$^{-/-}$*:Prkdc*$^{-/-}$) did not reduce the levels of IR-induced chromatin-bound RPA in G_2-arrested or cycling G_1 phase cells (Figure 4A and S4A). Similar results were obtained when analyzing *Lig4*$^{-/-}$*:Ku70*$^{-/-}$ abl pre-B cells (Figure 4B). The unique function of DNA-PK activity in promoting DNA end resection in G_0-arrested cells was confirmed with END-seq analysis of *AsiSI*-induced DSBs in *Lig4*$^{-/-}$ abl pre-B cells arrested in G_0 or G_2 and treated with or without DNA-PKcs inhibitor. Whereas G_0-arrested *Lig4*$^{-/-}$ abl pre-B cells treated with DNA-PKcs inhibitor exhibited significantly reduced END-seq signals in regions distal to the DSBs, the same treatment had little effect in cells arrested in G_2 phase of the cell cycle (Figure

253 4C and S4B). These results suggest that DNA-PK distinctly promotes DNA end resection

254 at DSBs in G_0 but not in other cell cycle phases.

255

Discussion

DNA end resection is one of the key events that determines whether cells utilize NHEJ, HR, or other repair pathways utilizing homologous sequences. During G_0 and G_1 phase of the cell cycle, NHEJ is the predominant DSB repair pathway and DNA end resection is largely limited compared to other phases of the cell cycle. However, in this study we revealed that DNA end resection dependent on CtIP and MRE11, which are required for resection in S and G_2 phases of the cell cycle, occurs at DSBs in G_0 mammalian cells (Figures 1B). In addition to CtIP and MRE11, we identified additional factors that promote resection in G_0 cells as components of the DNA-PK complex, including KU70, KU80 and DNA-PKcs, in a genome-wide CRISPR/Cas9 screen and showed that the kinase activity of DNA-PK is critical as resection of DSBs diminishes upon DNA-PKcs inhibitor treatment (Figures 2 and 3). Interestingly, we also found in our genome-wide CRISPR/Cas9 screen that inactivating FBXL12, the substrate recognition subunit of the SCF^{FBXL12} E3 ubiquitin ligase complex, promotes extensive resection of DNA ends in G_0 cells (Figure 3B). As the SCF^{FBXL12} E3 ubiquitin is thought to limit the abundance of the KU70/KU80 heterodimer (Postow and Funabiki 2013), our data are in line with the notion that loss of FBXL12 results in aberrant accumulation of KU70/KU80 at DSBs, and consequently elevated or prolonged activation of DNA-PK at DSBs which promotes resection in G_0 cells (Figure 5).

Why would resection occur in G_0 cells? Chemical modifications or secondary structures at DSBs have been identified as requiring DNA end processing to create a more accessible repair environment, which could presumably be the case at DSBs in G_0 cells (Weinfeld and Soderlind 1991). For example, Artemis is an endo and exonuclease

279 which is activated by DNA-PKcs and uses its nuclease activity to open DNA hairpins at
280 coding ends, which is required for V(D)J recombination, and cleaves 3' ssDNA overhangs
281 during NHEJ (Ma et al. 2002; Ma et al. 2005). Though Artemis was not identified in our
282 screen as having a role in G_0 DSB repair, it serves as an example of nuclease activity
283 being critical for DSB repair outside of HR. Interestingly, DNA end resection has a role in
284 recruiting anti-resection factors to limit extensive DNA end resection. The SHLD2
285 component of Shieldin binds ssDNA, suppresses RAD51 loading, and ultimately recruits
286 53BP1 to DSBs (Noordermeer et al. 2018). HELB, a 5'-3' DNA helicase, binds to RPA
287 and limits EXO1 and BLM-DNA2-mediated DNA end resection (Tkáč et al. 2016). Limited
288 DNA end resection in G_0 cells could be important in preventing extensive DNA end
289 resection. Altogether, we propose that DNA end resection in G_0 cells is likely not resulting
290 in aberrant HR but may be required to create more accessible DNA ends and/or to recruit
291 anti-resection factors.

292 Studies investigating the role of KU70/KU80 during DSB repair have found that
293 KU70/KU80 protects DSBs from nuclease activity. For example, at HO endonuclease
294 breaks in budding yeast, deletion of KU70/KU80 leads to ssDNA accumulation in G_1 cells
295 and increased MRE11 recruitment to DSBs compared to wild-type cells (Lee et al. 1998;
296 Clerici et al. 2008). Also in budding yeast, at inducible I-SceI DSBs, deletion of KU70
297 results in increased RFA1 foci formation in G_1, but deletion of NHEJ factor DNA Ligase
298 IV leads to no defect in RFA1 foci formation compared to wild-type cells, indicating that
299 KU70 itself, not NHEJ, is a barrier to DNA end resection (Barlow et al. 2008). In
300 mammalian cells, complementation of KU70/KU80 knockout cells with a *M. tuberculosis*
301 KU homolog persistently bound to DSBs in S phase results in reduced RPA and RAD51

foci formation after IR (Shao et al. 2012). Contrary to these roles for KU70/KU80 in protecting DNA ends from nucleolytic attack, we found that in G_0 cells, KU70/KU80 promotes DNA end resection (Figure 3A and 4B). We hypothesize that KU70/KU80 promotes resection through recruitment and activation of DNA-PKcs at DSBs (Gottlieb and Jackson 1993), as we also found that DNA-PKcs inhibition and genetic deletion of *Prkdc* leads to more RPA on chromatin after IR and more DNA end resection in G_0 cells (Figure 2C-E, S2C, S2D, 4A, 4C). It is important to note that most studies establishing the role of KU70/KU80 in protecting DNA ends were performed in *S. cerevisiae* which do not have a homolog to DNA-PKcs. Therefore, we hypothesize that the function of DNA-PK promoting DNA end resection in G_0 cells may not be evolutionarily conserved. Moreover, previous studies in *S. cerevisiae* and mammalian cells establishing DNA-PK as a pro-NHEJ complex did not analyze G_0 cells. We found that DNA-PK does not promote DNA end resection in G_1 or G_2 phase cells, only in G_0-arrested cells, indicating that DNA-PK-dependent DNA end resection is unique to G_0, but is not contradictory to its anti-resection function in G_1 or G_2 phase cells (Figure 4). In G_0 cells, KU70/KU80 could protect some DNA ends, but after recruitment and activation of DNA-PKcs, the net effect is DNA end resection. Additional studies may elucidate how the balance between DNA end protection and DNA end resection is regulated in G_0.

ATM and DNA-PK have been shown to have some overlapping functions in DNA damage response and repair, including phosphorylation of H2A.X in response to IR and signal join formation during V(D)J recombination (Stiff et al. 2004; Zha et al. 2011). However, we find that this is not the case during DNA end resection in G_0 cells as DNA-PK promotes resection in G_0 cells, but ATM does not have a detectable impact (Figure

S2B). ATM has been implicated in promoting HR repair by phosphorylating CtIP and promoting KU removal from DSBs, as well as phosphorylating DNA-PKcs at single-ended DSBs to remove it from these breaks that require DNA end resection (Wang et al. 2013; Britton et al. 2020). DNA-PKcs autophosphorylation promotes HR by removing it from DSBs to allow nuclease access, but is typically associated with promoting NHEJ by phosphorylating Artemis, XRCC4, and XLF (Zhou and Paull 2013; Bartlett and Lees-Miller 2018) So while ATM often promotes DNA end resection and HR, it appears that DNA-PKcs could be acting in place of ATM to promote DNA end resection in G_0 cells. It is additionally possible that DNA-PKcs phosphorylates a unique substrate(s) in G_0 cells that promotes DNA end resection.

In summary, we provide here evidence that DNA-PK promotes DNA end resection uniquely in G_0 cells, and that this DNA end resection is counteracted by FBXL12. We speculate that some aspects of DSB repair in G_0 function differently than DSB repair in cycling cells, and future studies may reveal the mechanism and utility of these key differences.

Figure 1

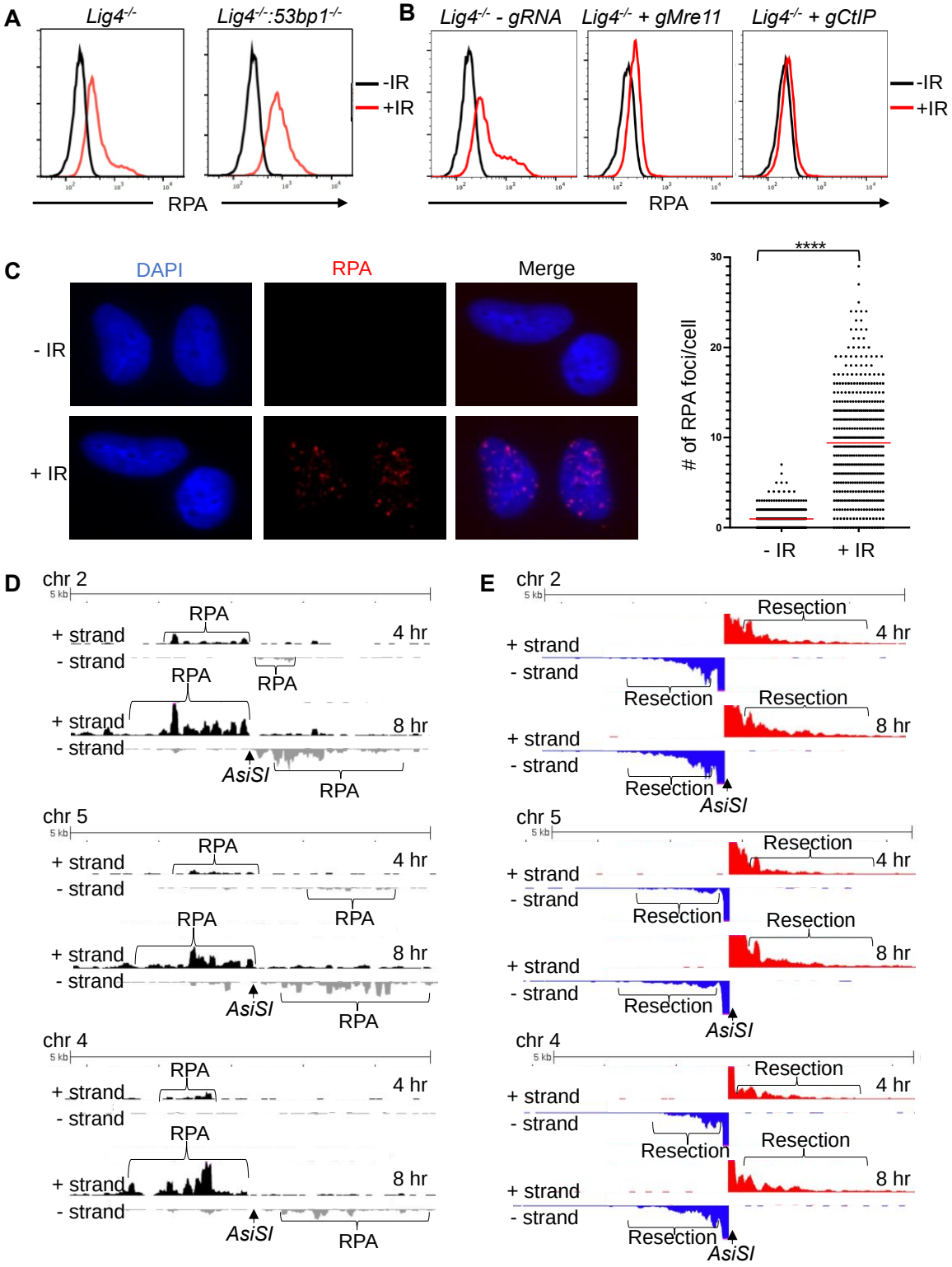

Figure 1. RPA is loaded onto ssDNA after DSBs in G_0 mammalian cells

(A) Flow cytometric analysis of chromatin-bound RPA in G_0-arrested *Lig4*$^{-/-}$ and *Lig4*$^{-/-}$ *:53bp1*$^{-/-}$ abl pre-B cells before and 3 hours after 20 Gray IR. Representative of three independent experiments. (B) Flow cytometric analysis of chromatin-bound RPA before and 2 hours after 15 Gy IR in G_0-arrested abl pre-B *Lig4*$^{-/-}$ cells (left), *Lig4*$^{-/-}$ cells depleted of *Mre11* (middle), and *Lig4*$^{-/-}$ cells depleted of *CtIP* (right). Representative of three independent experiments. (C) Representative images and quantification of IR-induced RPA foci from 3 independent experiments in G_0-arrested MCF10A cells before and 3 hours after 10 Gray IR. n=365 cells in No IR and n=433 cells in IR. Red bars indicate average number of RPA foci in No IR=0.96 and average number of RPA foci in IR=9.4 (****p<0.0001, unpaired t test). (D) RPA ChIP-seq tracks at *AsiSI* DSBs on chromosome 2, 5, and 4 at 4 hours (top) and 8 hours (bottom) after *AsiSI* endonuclease induction in G_0-arrested *Lig4*$^{-/-}$ abl pre-B cells. (E) Representative END-Seq tracks showing resection at *AsiSI* DSBs at chromosome 2, 5, and 4 at 4 hours (top) and 8 hours (bottom) after *AsiSI* induction in G_0-arrested *Lig4*$^{-/-}$ abl pre-B cells. END-seq data is representative from two independent experiments.

Figure S1

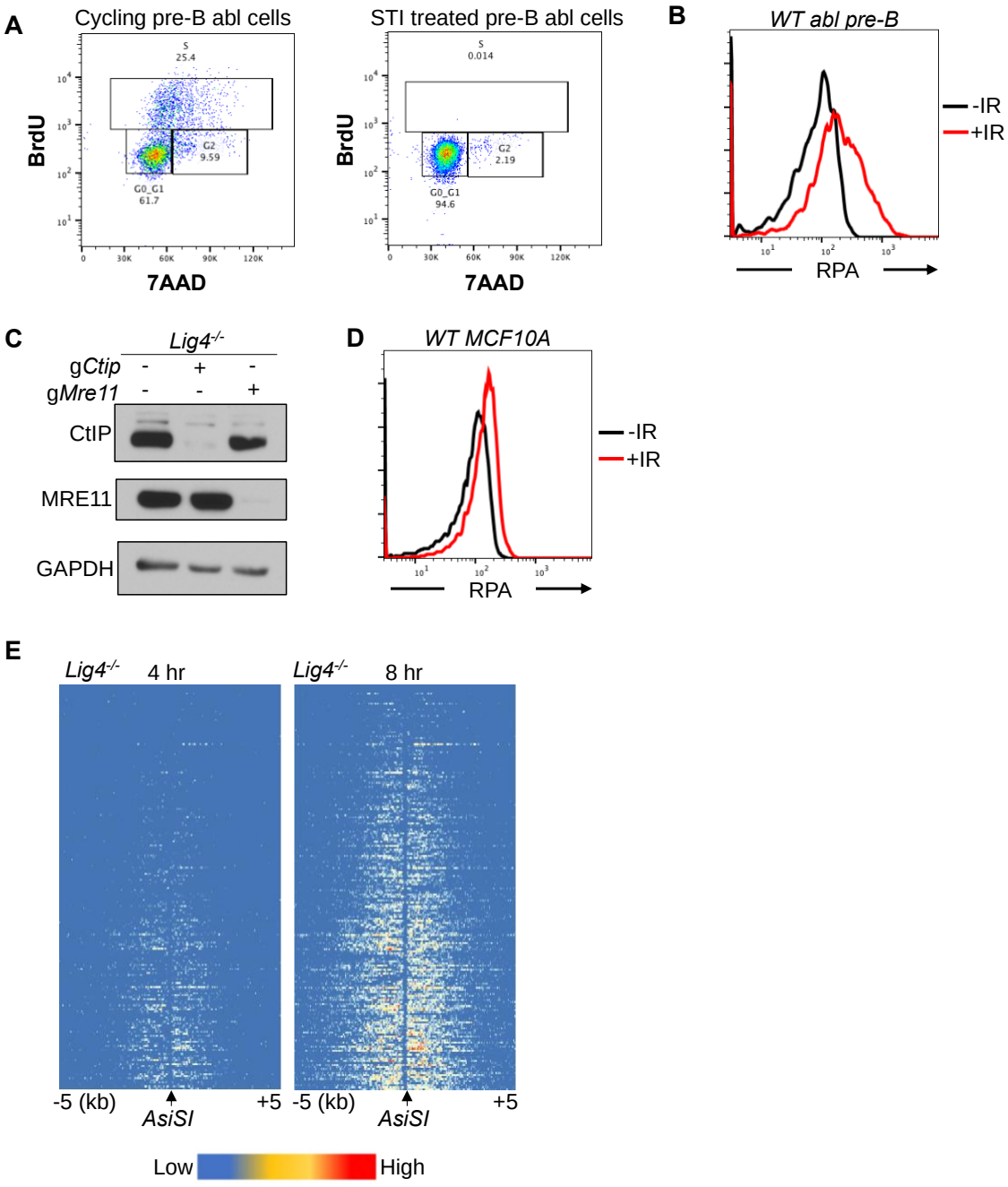

Figure S1. RPA is loaded onto ssDNA after DSBs in G_0 mammalian cells

(A) Flow cytometric analysis of cycling and STI treated *Lig4*$^{-/-}$ abl pre-B cells for BrdU content (y-axis) and DNA content (7AAD, x-axis). (B) Flow cytometric analysis of chromatin-bound RPA in wild-type G_0-arrested abl pre-B cells before and 3 hours after 20 Gray IR. (C) Western blot of bulk CtIP and MRE11 knockout in *Lig4*$^{-/-}$ abl pre-B cells (D) Flow cytometric analysis of chromatin-bound RPA loading in wild-type G_0-arrested MCF10A cells before and 3 hours after 20 Gray IR. (E) Heat maps of RPA ChIP-seq results at top 200 *AsiSI* sites in G_0-arrested *Lig4*$^{-/-}$ abl pre-B cells 4 hours (left) and 8 hours (right) after *AsiSI*-endonuclease induction.

Figure 2

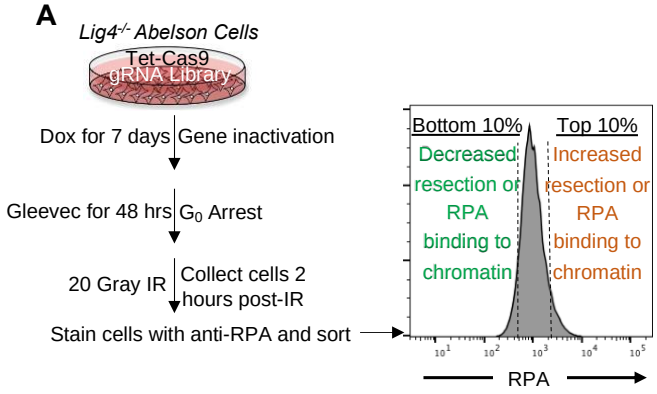

B

Gene	RPA Low Fold Enrichment	Gene	RPA High Fold Enrichment
Rbbp8	7,3,2,2,1	***Rnf168***	5,4,4,3,2
Nbn	5,5,4,3,2	***53bp1***	11,10,8,4,4
Prkdc	20,14,12,7,6	***Shld1***	6,5,4,4,3
Ku70	33,14,9,7,5	***Rif1***	5,4,2,2
Ku80	16,16,11,9,6	***Fbxl12***	64,33,26,22,20

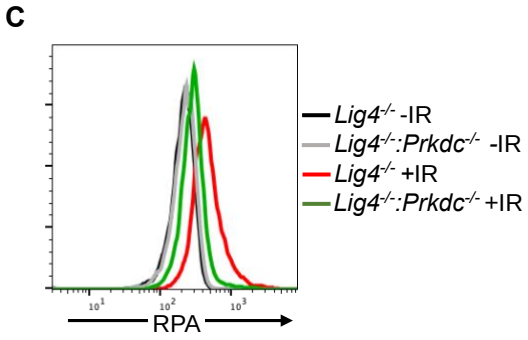

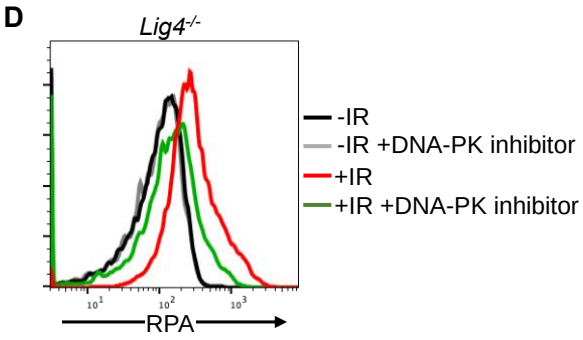

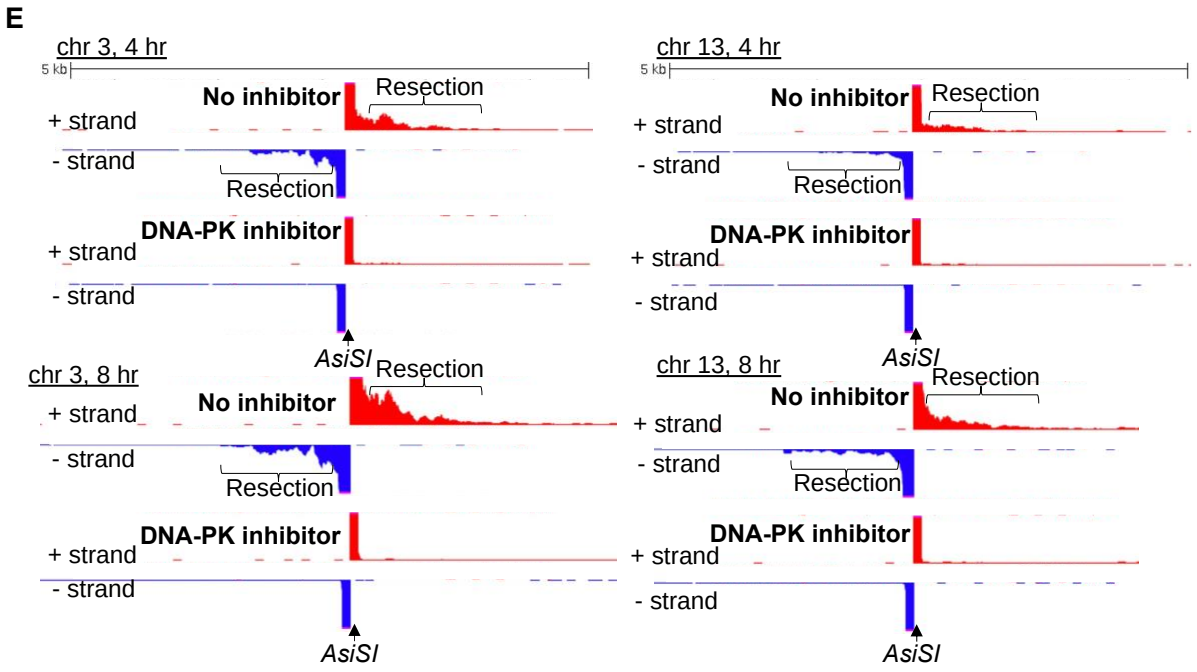

379
380

Figure 2. A genome-wide gRNA screen identifies DNA-PK as a factor that promotes DNA end resection in G_0

(A) Schematic of genome-wide guide RNA screen for factors promoting (low RPA) or inhibiting (high RPA) chromatin-bound RPA loading 2 hours after 20 Gray IR in G_0-arrested *Lig4*$^{-/-}$ abl pre-B cells. (B) Fold enrichment of selected guide RNAs in low RPA high RPA populations. (C) Flow cytometric analysis of chromatin-bound RPA in G_0-arrested *Lig4*$^{-/-}$ and *Lig4*$^{-/-}$*:Prkdc*$^{-/-}$ abl pre-B cells before and 3 hours after 15 Gray IR. Data is representative of three independent experiments in two different cell lines. (D) Flow cytometric analysis of chromatin-bound RPA in G_0-arrested *Lig4*$^{-/-}$ abl pre-B cells with and without 10 μm NU7441 (DNA-PKcs inhibitor) pre-treatment 1 hour before 20 Gray IR. Data is representative of three independent experiments in two different cell lines. (E) Representative END-seq tracks at chromosome 3 (left) and chromosome 13 (right) in G_0-arrested *Lig4*$^{-/-}$ abl pre-B cells 4 hours (top) and 8 hours (bottom) after *AsiSI* DSB induction, with and without 10 μm NU7441 treatment.

Figure S2

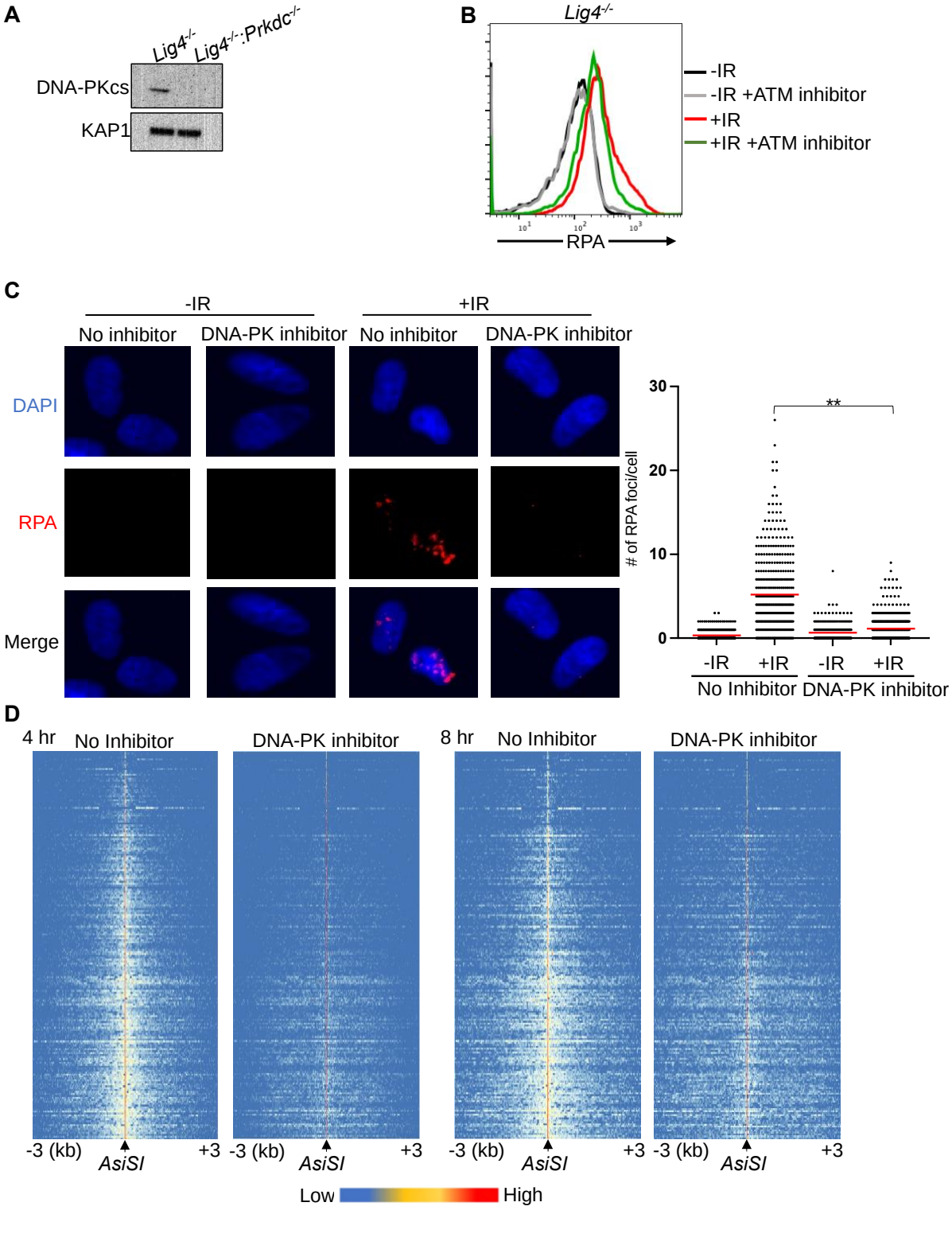

Figure S2. A genome-wide gRNA screen identifies DNA-PK as a factor that promotes DNA end resection in G_0

(A) Western blot analysis of DNA-PKcs protein in *Lig4*$^{-/-}$ and *Lig4*$^{-/-}$*:Prkdc*$^{-/-}$ abl pre-B cells. (B) Flow cytometric analysis of chromatin-bound RPA in G_0-arrested abl pre-B cells with and without 1 hour pre-treatment with 15 μm KU-55933 (ATM inhibitor), before and 3 hours after 20 Gray IR. (C) Representative images and quantitation from 3 independent experiments of IR-induced RPA foci in G_0-arrested MCF10A cells with and without 10 μm NU7441, before and 3 hours after 10 Gray IR. For No Inhibitor -IR condition, n=426, average number of RPA foci=0.34. For No Inhibitor +IR condition, n=389, average number of RPA foci=5.2. For DNA-PK inhibitor treated -IR condition, n=266, average number of RPA foci=0.66. For DNA-PK inhibitor treated +IR condition, n=441, average number of RPA foci=1.13. Red bar indicates mean number of RPA foci (**p=0.003). (D) Heat maps of END-seq at top 200 *AsiSI* DSBs with and without 10 μm NU7441 treatment in G_0-arrested *Lig4*$^{-/-}$ abl pre-B cells 4 hours (left) and 8 hours (right) after *AsiSI* DSB induction.

Figure 3

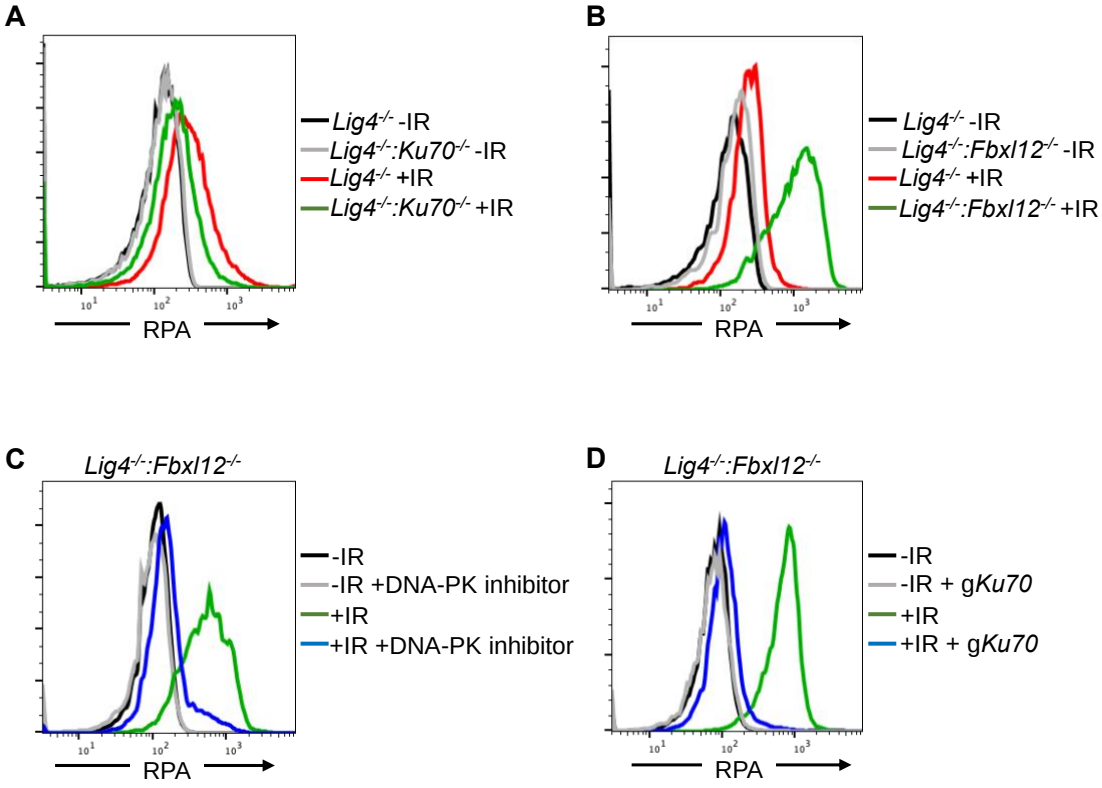

425
426
427
428

Figure 3. FBXL12 inhibits KU70/KU80-promoted DNA end resection

(A) Flow cytometric analysis of chromatin-bound RPA in G_0-arrested *Lig4*$^{-/-}$ abl pre-B cells vs *Lig4*$^{-/-}$*:Ku70*$^{-/-}$ abl pre-B cells before and 3 hours after 20 Gray IR. Data is representative of three independent experiments in two different cell lines. (B) As in A, in G_0-arrested *Lig4*$^{-/-}$ and *Lig4*$^{-/-}$*:Fbxl12*$^{-/-}$ abl pre-B cells. Data is representative of three independent experiments in at least two different cell lines. (C). Flow cytometric analysis of chromatin-bound RPA in G_0-arrested *Lig4*$^{-/-}$*:Fbxl12*$^{-/-}$ abl pre-B cells with and without 10 μm NU7441 treatment, before and 3 hours after 20 Gray IR. Data is representative of three independent experiments in at least two different cell lines (D) Flow cytometric analysis of chromatin-bound RPA in G_0-arrested *Lig4*$^{-/-}$*:Fbxl12*$^{-/-}$ abl pre-B cells before and after KU70 knockout, before and 3 hours after 15 Gray IR. Data is representative of three independent experiments.

Figure S3

A

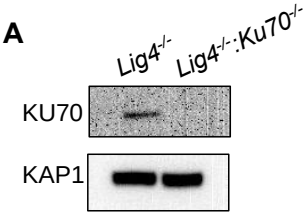

B

FBXL12 reference sequence (gRNA sequence in red):
395th to 492nd nucleotide of exon 4
TGCCGGCCTTTCGCGATGAGCATCTGCAGGGCCTTACCCGATTCCGAGCCCTGCGCTCGCTGGT
GCTGGGCGGCACCTACCGGGTCACTGAGACCGGG

Point Mutation
Insertion

Allele 1:
TGCCGGCCTTCCGGG (69 nt deletion) TCACTGAGACCGGG
Allele 2:
TGCCGGCCTTCCGC*A*GATG (41 nt deletion)
CTGGTGCTGGGCGGCACCTACCGGGTCACTGAGACCGGG

C

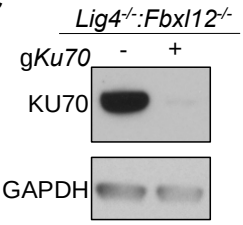

Figure S3. FBXL12 inhibits KU70/KU80-promoted DNA end resection

(A) Western blot analysis of KU70 protein in *Lig4-/-* and *Lig4-/-:Ku70-/-* abl pre-B cells.

(B) Gene sequence of *Lig4*$^{-/-}$*:Fbxl12*$^{-/-}$ abl pre-B cell clones indicating deletions. (C) Western blot analysis of KU70 protein in *Lig4*$^{-/-}$*:Fbxl12*$^{-/-}$ abl pre-B cells.

Figure 4

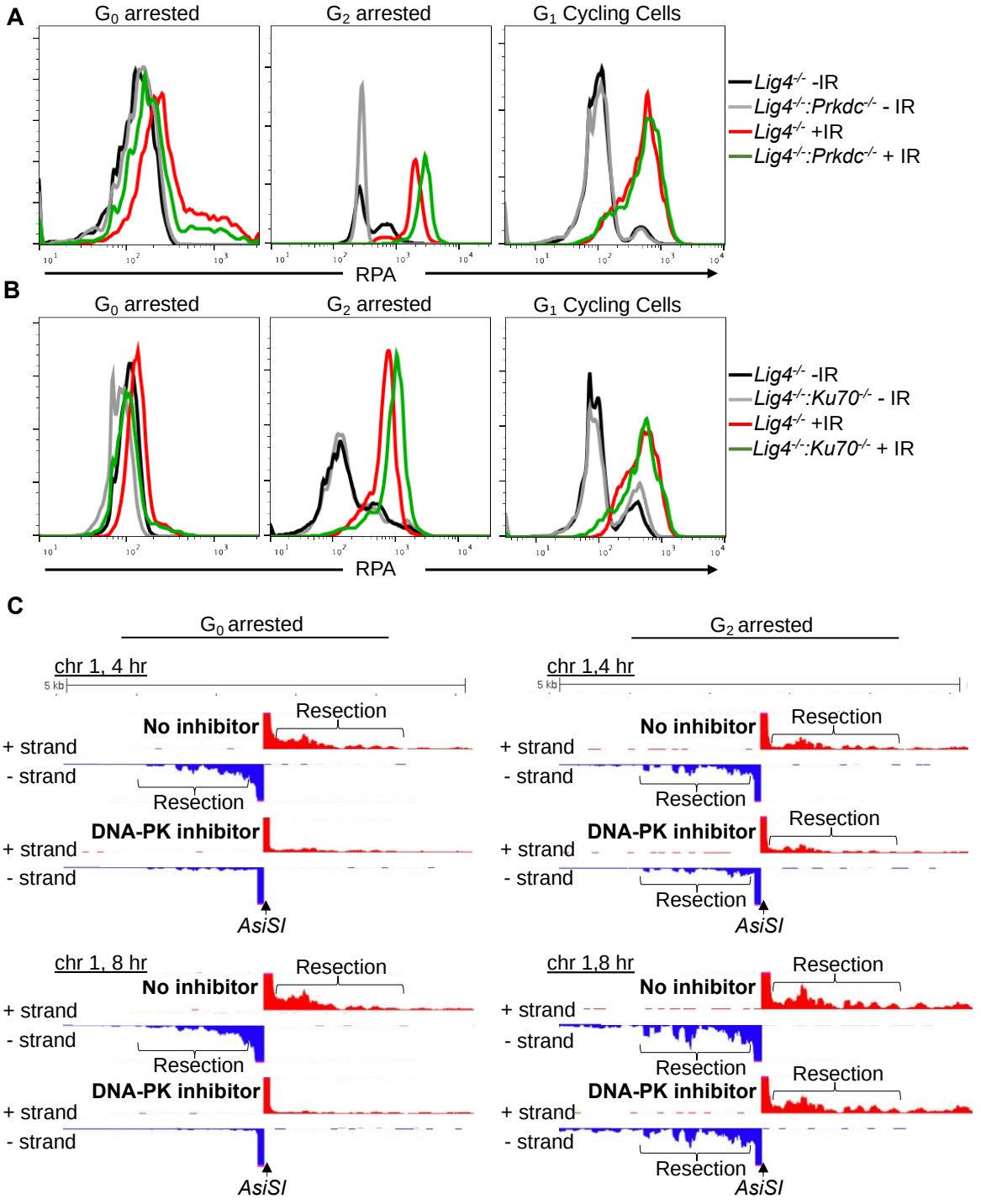

458 **Figure 4. DNA-PK mediates DNA end resection in G_0 but not G_1 or G_2**

459 (A) Flow cytometric analysis of chromatin-bound RPA in *Lig4*$^{-/-}$ and *Lig4*$^{-/-}$*:Prkdc*$^{-/-}$ abl pre-
460 B cells arrested in G_0 (left), arrested in G_2 by 10 μm RO-3306 treatment for 16 hours and
461 gated on 4N (middle), and G_1 cells gated on 2N DNA content in cycling cells (right), before
462 and 3 hours after 20 Gray IR. Data is representative of three independent experiments in
463 at least two different cell lines. (B) As in A in *Lig4*$^{-/-}$ and *Lig4*$^{-/-}$*:Ku70*$^{-/-}$ abl pre-B cells. (C)
464 Representative END-seq tracks in G_0 (left) and G_2-arrested (right, by 10 μm RO-3306
465 treatment for 16 hours) *Lig4*$^{-/-}$ abl pre-B cells, with and without 10 μm NU7441 treatment
466 on chromosome 1, 4 hours (top) and 8 hours (bottom) after *AsiSI* endonuclease induction.
467
468
469
470
471
472
473
474
475
476
477
478
479

Figure S4

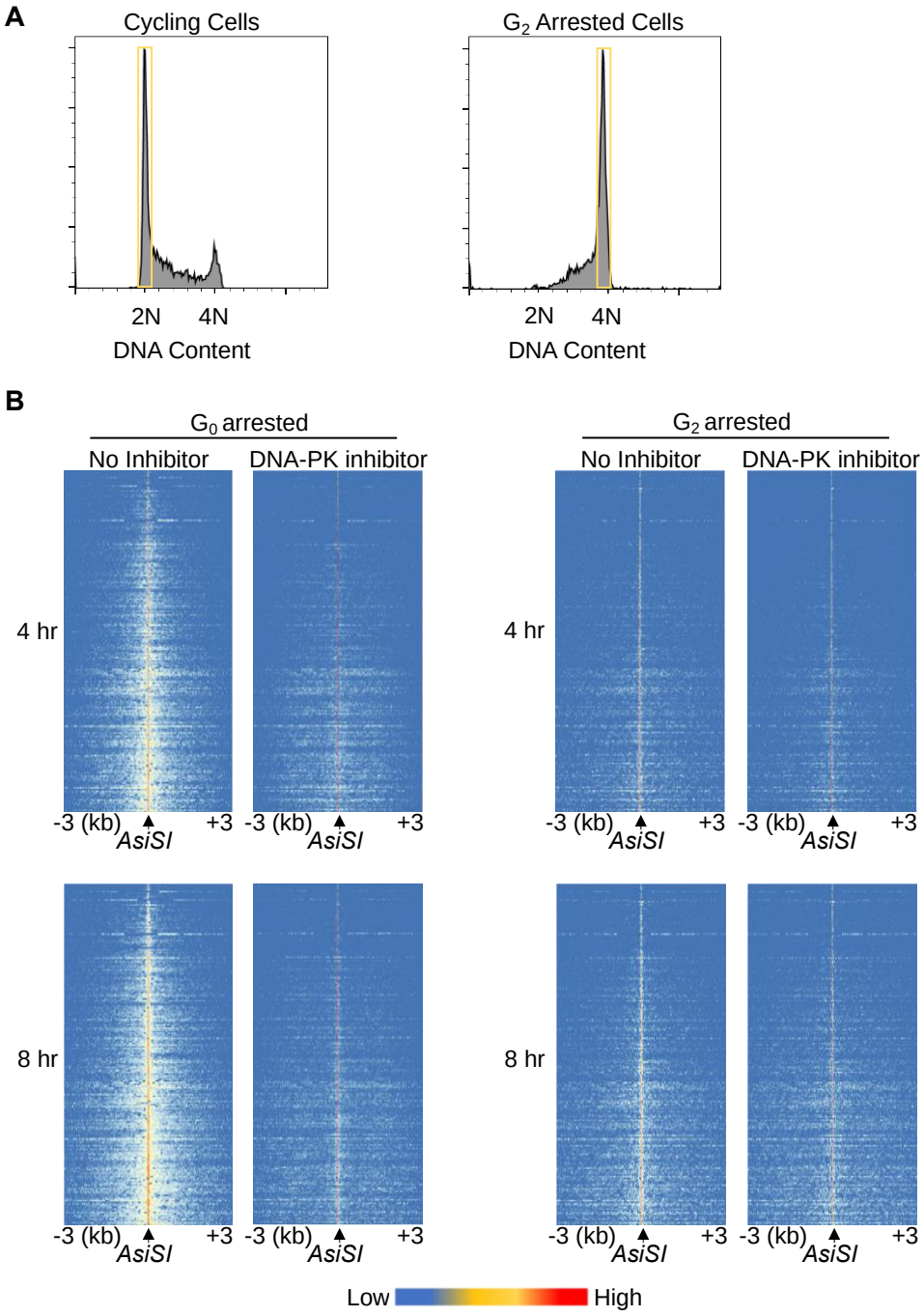

Figure S4. DNA-PK mediates DNA end resection in G_0 but not G_1 or G_2

(A) Flow cytometric analysis of DNA content (7AAD) in RO-3306 treated (right) and cycling cells (left) showing gating used for RPA flow cytometry analysis. (B) Heat maps of END-seq at top 200 *AsiSI* DSBs in G_0-arrested *Lig4*$^{-/-}$ abl pre-B (left) and G_2-arrested *Lig4*$^{-/-}$ abl pre-B (right) 4 hours (top) and 8 hours (bottom) after *AsiSI* DSB induction, with and without 10 μm NU7441 treatment.

Figure 5

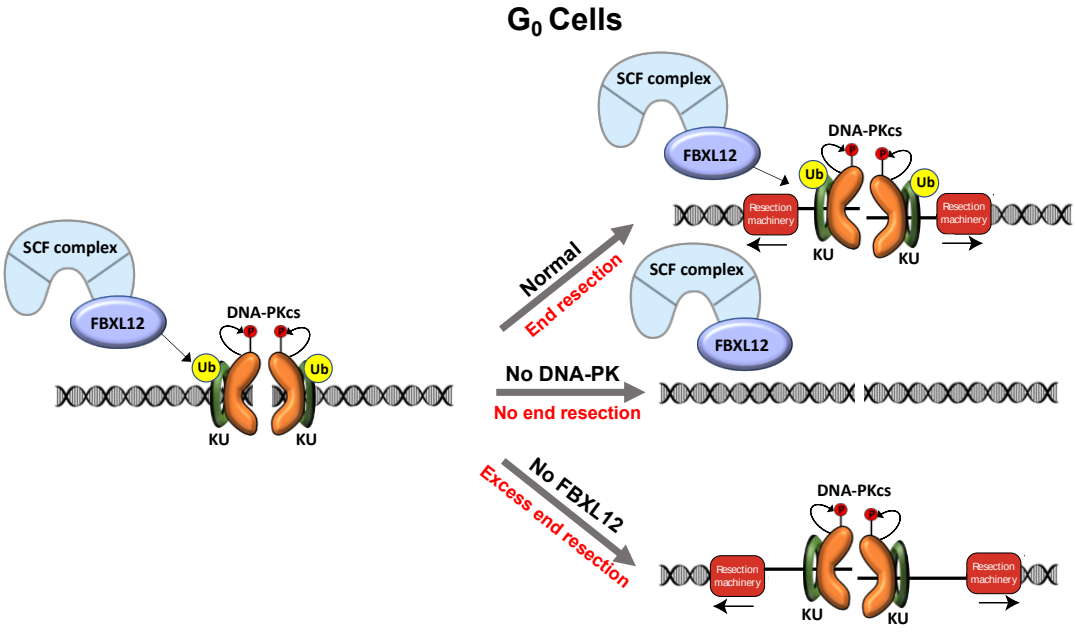

Figure 5. Model of DNA-PK-mediated DNA end resection in G_0 cells

Normally in G_0 at DSBs, the DNA-PK complex promotes DNA end resection. This resection is counteracted by FBXL12. Without DNA-PK, there is no DNA end resection in G_0. Without FBXL12, DNA-PK persists at DSBs which leads to more extensive DNA end resection.

Materials and Methods

Key Resources Table

Reagent type (species) or resource	Designation	Source or reference	Identifiers	Additional information
Antibody	Anti-CtIP (Rabbit polyclonal)	N/A	custom made (Richard Baer, Columbia University)	WB (1:1000)
Antibody	Anti-MRE11 (Rabbit polyclonal)	Novus Biologicals	NB100-142 RRID:AB_11093 76	WB (1:2000)
Antibody	Anti-GAPDH (GAPDH-71.1) (Mouse monoclonal)	Millipore Sigma	G8795 RRID:AB_10789 91	WB (1:10000)
Antibody	Anti-KAP1 (N3C2) (Rabbit polyclonal)	Genetex	GTX102226 RRID:AB_2037324	WB (1:2000)
Antibody	Anti-RPA32 (4E4) (Rat monoclonal)	Cell Signaling Technology	2208S RRID:AB_2238543	WB (1:1000) FC (1:200) IF (1:500)
Antibody	Anti-KU70 (D10A7) (Rabbit monoclonal)	Cell Signaling Technology	4588S RRID:AB_11179211	WB (1:1000)
Antibody	Anti-DNA-PK (SC57-08) (Rabbit monoclonal)	Invitrogen	MA5-32192 RRID:AB_28094 79	WB (1:1000)
Antibody	Anti-RPA32	Abcam	ab10359 RRID:AB_29709 5	ChIP (10 ug)
Antibody	HRP, goat anti-mouse	Promega	W4021 RRID:AB_430834	WB (1:5000)
Antibody	HRP, goat anti-rabbit IgG	Promega	W4011 RRID:AB_430833	WB (1:5000)
Antibody	Alexa Fluor 488, goat anti-rat IgG	BioLegend	405418 RRID:AB_2563120	FC (1:500)

Antibody	Alexa Fluor 647, goat anti-rat IgG	BioLegend	405416 RRID:AB_2562967	FC (1:500)
Antibody	Alexa Fluor 594, goat anti-rat IgG	BioLegend	405422 RRID:AB_2563301	IF (1:500)
Recombinant DNA	pCW-Cas9 (plasmid)	Addgene	50661 RRID:Addgene_50661	
Recombinant DNA	pKLV-U6 gRNA(BbsI)-PGKpuro-2ABFP (plasmid)	Addgene	50946 RRID:Addgene_50946	
Recombinant DNA	Genome-wide CRISPR guide RNA library V2 (plasmid)	Addgene	67988 RRID:Addgene_67988	
Cell line (*H. sapiens*)	*MCF10A*	ATCC	CRL-10317 RRID:CVCL_0598	
Cell line (*H. sapiens*)	*MCF10A:iCas9*	This study	Clone 25	Available upon request
Cell line (*M. musculus*)	WT:*iCas9* abl pre-B cells	This study	M63.1.MG36.iCas9.302	Available upon request
Cell line (*M. Musculus*)	*Lig4*$^{-/-}$*:iCas9* abl pre-B cells	This study	A5.83.MG9.iCas9.16	Available upon request
Cell line (*M. Musculus*)	*Lig4*$^{-/-}$*:iCas9* abl pre-B cells	This study	A5.115.iCas9.72	Available upon request
Cell line (*M. Musculus*)	*Lig4*$^{-/-}$*:53bp1:iCas9* abl pre-B cells	This study	Clone 82	Available upon request
Cell line (*M. musculus*)	*Lig4*$^{-/-}$*:Ku70*$^{-/-}$*:iCas9* abl pre-B cells	This study	Clones 134 and 140	Available upon request
Cell line (*M. musculus*)	*Lig4*$^{-/-}$*:Prkdc*$^{-/-}$*:iCas9* abl pre-B cells	This study	Clone 6	Available upon request
Cell line (*M. musculus*)	*Lig4*$^{-/-}$*:Fbxl12*$^{-/-}$*:iCas9* abl pre-B cells	This study	Clone 6	Available upon request
Cell line (*M. musculus*)	*Lig4*$^{-/-}$*:iAsiSI* abl pre-B cells	This study	Clone 20	Available upon request
Chemical compound, drug	Imatinib	Selleckchem	S2475	

Chemical compound, drug	Doxycycline	Sigma-Aldrich	D9891	
Chemical compound, drug	Polybrene	Sigma Aldrich	S2667	
Chemical compound, drug	Lipofectamine 2000	Thermo Fisher Scientific	11668019	
Chemical compound, drug	NU7441	Selleck Chemicals	S2638	
Chemical compound, drug	KU-55933	Selleck Chemicals	S1092	
Chemical compound, drug	EGF	PeproTech	AF-100-15	
Chemical compound, drug	Hydrocortisone	Sigma-Aldrich	H-0888	
Chemical compound, drug	Cholera Toxin	Sigma-Aldrich	C-8052	
Chemical compound, drug	Insulin	Sigma-Aldrich	I-1882	
Commercial assay or kit	7-AAD (DNA stain)	BD Biosciences	559925 RRID:AB_2869266	
Commercial assay or kit	Cytofix/Cytoperm solution	BD Biosciences	554722 RRID:AB_2869010	
Commercial assay or kit	Perm/Wash Buffer	BD Biosciences	554723 RRID:AB_2869011	
Commercial assay or kit	FITC BrdU Flow Kit	BD Biosciences	559619 RRID:AB_2617060	
Sequence-based reagent	pKLV lib330F	This study (designed based on (Tzelepis et al. 2016))	PCR primers	AATGGACTATCATATGCTTACCGT
Sequence-based reagent	pKLV lib490R	This study (designed based on (Tzelepis et al. 2016)	PCR primers	CCTACCGGTGGATGTGGAATG
Sequence-based reagent	PE.P5_pKLV lib195 Fwd	This study (designed based on (Tzelepis et al. 2016) and standard Illumana adaptor sequences)	PCR primers	AATGATACGGCGACCACCGAGATCTGGCTTTATATATCTTGTGGAAAGGAC

Sequence-based reagent	P7 index180 Rev	This study (designed based on (Tzelepis et al. 2016) and standard Illumana adaptor sequences)	PCR primers	CAAGCAGAAGAC GGCATACGAGAT *INDEX*GTGACTG GAGTTCAGACGT GTGCTCTTCCGA TCCAGACTGCCT TGGGAAAAGC
Sequence-based reagent	BU1	(Canela et al. 2016)	PCR primers	5′-Phos-GATCGGAAGAG CGTCGT GTAGGGAAAGA GTGUU[Biotin-dT]U [Biotin-dT]UUACACTCTT TC CCTACACGACGC TCTTCCGATC* T-3′ [*phosphorothioate bond]
Sequence-based reagent	BU2	(Canela et al. 2016)	PCR primers	5′-Phos-GATCGGAAGAG CACACG TCUUUUUUUUAG ACGTGTGCTCTT CCGATC*T-3′ [*phosphorothioate bond]
Sequence-based reagent	*53bp1* gRNA sequence	Sequence is from (Tzelepis et al. 2016)	N/A	GAACCTGTCAGA CCCGATC
Sequence-based reagent	*Ctip* gRNA sequence	Sequence is from (Tzelepis et al. 2016)	N/A	ATTAACCGGCTA CGAAAGA
Sequence-based reagent	*Mre11 gRNA sequence*	Sequence is from (Tzelepis et al. 2016)	N/A	TGCCGTGGATAC TAAATAC
Sequence-based reagent	*Prkdc gRNA sequence*	Sequence is from (Tzelepis et al. 2016)	N/A	ATGCGTCTTAGG TGATCGA
Sequence-based reagent	*Ku70 gRNA sequence*	Sequence is from (Tzelepis et al. 2016)	N/A	CCGAGACACGG TTGGCCAT
Sequence-based reagent	*Fbxl12 gRNA sequence*	Sequence is from (Tzelepis et al. 2016)	N/A	TTCGCGATGAGC ATCTGCA
Software, algorithm	Image J	NIH	RRID:SCR_003070	

Software, algorithm	FlowJo	FlowJo	RRID:SCR_008520	
Software, algorithm	Prism	GraphPad	RRID:SCR_002798	
Software, algorithm	Gen5	Biotek Instruments	RRID:SCR_017317	
Software, algorithm	SeqKit	(Shen et al. 2016)	RRID:SCR_018926	
Software, algorithm	Bowtie	(Langmead et al. 2009)	RRID:SCR_005476	
Software, algorithm	SAMtools	(Li et al. 2009a)	RRID:SCR_002105	
Software, algorithm	BEDtools	(Quinlan and Hall 2010)	RRID:SCR_006646	
Other	LSRII Flow cytometer	BD Bioscience	RRID:SCR_002159	
Other	FACS Celesta Flow Cytometer	BD Bioscience	RRID:SCR_019597	
Other	FACSAria II Cell Sorter	BD Bioscience	RRID:SCR_018934	
Other	Lionheart LX automated microscope	BioTex Instruments	RRID:SCR_019745	
Other	4-D Amaxa Nucleofecter	Lonza	NA	

Cell Lines and Maintenance

Abelson virus-transformed pre-B cell lines were maintained in DMEM (Thermo Fisher #11960-077) supplemented with 10% fetal bovine serum, 1% Penicillin-Streptomycin, 2 mM glutamine, 1 mM sodium pyruvate, 1X nonessential amino acids, and 0.4% beta-mercaptoethanol at 37°C with 5% CO_2. MCF10A cells were maintained in DMEM/F12 (Gibco, #11330032), 5% horse serum, 20 ng/mL EGF, 0.5 μg/mL hydrocortisone, 100 ng/mL cholera toxin, 10 μg/mL insulin, and 1% Penicillin-Streptomycin at 37°C with 5%

CO_2. 293T cells were maintained in DMEM (Corning, #10-013-CM) supplemented with 10% fetal bovine serum and 1% Penicillin-Streptomycin at 37°C with 5% CO_2.

Lig4$^{-/-}$ abl pre-B cells contain pCW-Cas9 (addgene, #50661) which expresses cas9 under a doxycycline-induced promoter. To generate single cell clones of *Lig4*$^{-/-}$*:53bp1*$^{-/-}$, *Lig4*$^{-/-}$*:Ku70*$^{-/-}$, *Lig4*$^{-/-}$*:Prkdc*$^{-/-}$, and *Lig4*$^{-/-}$*:Fbxl12*$^{-/-}$, guide RNAs (gRNAs) against each gene were cloned into pKLV-U6gRNA-EF(BbsI)-PGKpuro2ABFP (addgene, #62348) modified to express human CD2 as a cell surface marker. *Lig4*$^{-/-}$ abl pre-B cells were grown in 3 μg/mL of doxycycline for 2 days and then nucleofected with the pKLV-gRNA plasmid using a Lonza Amaxa Nucleofector. The next day, cells were magnetically selected for human CD2 cell surface expression, and selected cells were grown in 3 μg/mL doxycycline overnight. Serial dilution in 96 well plates was used to isolate single cells. After cell growth, potential clones were confirmed to have the gene of interest knocked out by Sanger sequencing or western blotting.

Bulk gene inactivation

gRNAs against *Mre11*, *CtIP*, and *Ku70* were cloned into pKLV-U6gRNA-EF(BbsI)-PGKpuro2ABFP (addgene, #62348). 293T cells were transfected with the pKLV-gRNA plasmid along with lentiviral packaging and lentiviral envelope plasmids. 3 days post-transfection, supernatant containing pKLV-gRNA lentivirus was filtered with a 0.45 micron filter. *Lig4*$^{-/-}$ cells were resuspended in the filtered viral supernatant supplemented with 5 μg/mL polybrene (Sigma-Aldrich, #S2667) in 6-well plates and centrifuged at 1,800 RPM for 1.5 hrs at room temperature. After spin infection, virally transduced cells were supplemented with DMEM containing 3 μg/mL doxycycline for 3

days before flow cytometry-assisted cell sorting or magnetic-assisted cell sorting based on hCD2 cell surface expression.

Flow Cytometry

Abl pre-B cells were arrested in G_0 using 3 μM imatinib (Selleck Chemicals, #S2475) for 48 hours. MCF10A cells were arrested in G_0 by withdrawing EGF for 48 hours. To arrest cells in G_2, abl pre-B cells were treated with 10 μM RO-3306 (Selleck Chemicals, #S7747) overnight. For experiments analyzing DNA-PKcs and ATM inhibition, 10 μM NU7441 (Selleck Chemicals, #S2638) or 15 μM KU-55933 (Selleck Chemicals, #S1092) was added 1 hour prior to irradiation. After irradiation with 20 Gray, cells were allowed to recover for 3 hours. Cells were then pre-extracted with 0.05% Triton-X (STI-treated abl pre-B cells), 0.2% Triton-X (proliferating abl pre-B cells) or 0.5% Triton-X (MCF10A cells) in PBS and fixed with BD Cytofix/Cytoperm solution (BD Biosciences, #554722) containing 4.2% formaldehyde. Fixed cells were stained with anti-RPA32 (Cell Signaling Technology, #2208S) for 2 hours at room temperature, and then treated with a fluorescent conjugated secondary antibody (BioLegend, #405416 or BioLegend, #405418) for 1 hour at room temperature. 7-AAD was added to each sample to stain for DNA content. Cells were analyzed using a BD LSRII Flow Cytometer or a BD FACSCelesta and flow cytometry results were further analyzed using FlowJo.

Nuclear RPA Immunofluorescence Staining

60,000 G_0-arrested MCF10A cells grown on cover slips were irradiated with 10 Gray and then allowed to recover for 3 hours at 37°C with 5% CO_2. Cells were then washed with PBS containing 0.1% Tween-20 (PBST), pre-extracted using cold 0.5% Triton-X in PBS for 5 minutes, fixed with 4% formaldehyde for 15 minutes, and blocked in 3% BSA-

PBST for 1 hour at room temperature. Cells were incubated overnight at 4°C in primary antibody (anti-RPA32, Cell Signaling Technology, #2208). diluted in 3% BSA-PBST Samples were then washed 3x with PBST, incubated with secondary antibody diluted in 3% BSA (Alexa Fluor 594 Goat anti-Rat IgG, BioLegend, #405422) in the dark for 1 hr at room temperature, washed 3x with PBST, and mounted in Prolong Gold Antifade Mountant with DAPI (Life Technologies, #P-36931). Images were taken using a Biotek Lionheart Automatic Microscope and foci quantification was performed using Biotek Gen5 software.

END-Seq and RPA ChIP-Seq

Sequencing assays were performed in *Lig4*$^{-/-}$ abl pre-B cells after arrest in G_0 with imatinib for 24 hours or arrest in G_2 with RO-3306 for 12 hours, then treated with doxycycline for 24 hours followed by tamoxifen treatment for 4 or 8 hours to induce AsiSI breaks in the nucleus. End-seq was performed as previously described (Canela et al. 2016; Chen et al. 2021a; Wong et al. 2021). Cells were embedded in agarose plugs, lysed, and treated with proteinase K and RNase A. The DNA was then blunted with ExoVII (NEB) and ExoT (NEB), A-tailed, and ligated with a biotinylated hairpin adaptor. DNA was then recovered and sonicated to a length between 150 and 200 bp and biotinylated DNA fragments were purified using streptavidin beads (MyOne C1, Invitrogen). The DNA was then end-repaired and ligated to hairpin adaptor BU2 and amplified by PCR. RPA single-strand DNA sequencing was performed as previously described (Paiano et al. 2021). Cells were fixed in 1% formaldehyde (Sigma, F1635) for 10 min at 37°C, quenched with 125 mM glycine (Sigma), washed twice with cold 1× PBS. After centrifugation, pellets were frozen on dry ice, and stored at −80°C. Sonication, immunoprecipitation, and library preparation

were performed as previously detailed (Tubbs et al. 2018). Before immunoprecipitation, sheared chromatin was precleared with 40 µL of Dynabeads Protein A (Thermo Fisher) for 30 min at 4°C. Sheared chromatin was enriched with 10 µg of anti-RPA32/RPA2 antibody (Abcam, ab10359) on Dynabeads Protein A overnight at 4°C. During library preparation, kinetic enrichment of single-strand DNA was performed by heating sheared DNA for 3 min at 95°C and allowing DNA to return to room temperature (Tubbs et al. 2018). All END-seq and RPA ChIP-seq libraries were collected by gel purification and quantified using qPCR. Sequencing was performed on the Illumina NextSeq500 (75 cycles) as previously described (Chen et al. 2021a).

Genome Alignment and Visualization

END-seq and RPA ChIP-seq single-end reads were aligned to the mouse genome (mm10) using Bowtie v1.1.2 (Langmead et al. 2009) with parameters (-n 3 -k 1 -l 50) for END-seq and (-n 2 -m 1 -l 50) for RPA ChIP-seq. All plots or analysis were done for the top 200 *AsiSI* sites determined by END-seq. Alignment files were generated and sorted using SAMtools (Li et al. 2009b) and converted to bedgraph files using bedtools genomecov (Quinlan and Hall 2010) following by bedGraphToBigWig to make a bigwig file (Kent et al. 2010). Visualization of genomic profiles was done by the UCSC genome browser (Kent et al. 2002) and normalized to present RPM. Heat maps were produced using the R package pheatmap.

Guide RNA Library Screen

144 million *Lig4*$^{-/-}$ abl pre-B cells were transduced with a viral tet-inducible guide RNA library (Pooled Library #67988, Addgene) containing 90,000 gRNAs targeting over 18,000 mouse genes. 3 days post-infection, cells were sorted for gRNA vector

598 expression using a BD FACSAria flow assisted cell sorter. The next day, sorted cells
599 were treated with 3 µg/ml doxycycline to induce gRNA expression. 7 days later, cells
600 were treated with Gleevec to arrest cells in G_0. 48 hours later, cells were irradiated with
601 20 Gray and allowed to recover for 2 hours. After collection, cells were permeabilized,
602 fixed, and stained with anti-RPA32 in the same manner as described in the Flow
603 Cytometry section. After staining, the top 10% and bottom 10% of RPA stained cells
604 were collected using flow assisted cell sorting and genomic DNA was extracted. An
605 Illumina sequencing library was generated using two rounds of PCR to amplify the
606 gRNA and add a barcode, then purified PCR products containing the barcoded enriched
607 gRNAs were sequenced on an Illumina HiSeq2500. Sequencing data were processed
608 as previously described (Chen et al. 2021a).

609 **Western Blotting**

610 The following antibodies were used for western blot analysis: CtIP (gift from Dr. Richard
611 Baer, [Columbia University, New York], 1:1000), MRE11 (Novus Biologicals, NB100-
612 142, 1:2000), GAPDH (Sigma, G8795, 1:10,000), DNA-PK (Invitrogen, MA5-32192,
613 1:1000), KAP1 (Genetex, GTX102226, 1:2000), KU70 (Cell Signaling Technology,
614 #4588, 1:1000).

615 **Plasmid Constructs**

616 pCW-Cas9 was a gift from Eric Lander and David Sabatini (Addgene plasmid #50661)
617 (Wang et al. 2014). pKLV-U6gRNA(BbsI)-PGKpuro2ABFP was a gift from Kosuke Yusa
618 (Addgene plasmid #50946) (Koike-Yusa et al. 2014). Mouse Improved Genome-wide
619 Knockout CRISPR Library v2 was a gift from Kosuke Yusa (Addgene #67988) (Tzelepis
620 et al. 2016).

Acknowledgements

The authors thank Chitra Mohan for designing the model graphic and Yinan Wang for performing the bioinformatics for the high throughput screen. We thank the Weill Cornell Flow Cytometry Core for flow cytometry and thank the Weill Cornell Epigenomics Core for providing advice and performing the sequencing for the high throughput screen. JKT is supported by NIH R35 GM139816 and R01 CA95641. BPS is supported by NIH R01 AI047829 and R01 AI074953. FCF is supported by NIH F31 CA239442. JKT and BPS were also supported by the Starr Cancer Consortium and Emerson Collective Cancer Research Fund.

References

Averbeck NB, Ringel O, Herrlitz M, Jakob B, Durante M, Taucher-Scholz G. 2014. DNA end resection is needed for the repair of complex lesions in G1-phase human cells. *Cell Cycle* **13**: 2509-2516.

Barlow JH, Lisby M, Rothstein R. 2008. Differential regulation of the cellular response to DNA double-strand breaks in G1. *Mol Cell* **30**: 73-85.

Bartlett EJ, Lees-Miller SP. 2018. Established and Emerging Roles of the DNA-Dependent Protein Kinase Catalytic Subunit (DNA-PKcs). in *Targeting the DNA Damage Response for Anti-Cancer Therapy* (eds. J Pollard, N Curtin), pp. 315-338. Springer International Publishing, Cham.

Biehs R, Steinlage M, Barton O, Juhász S, Künzel J, Spies J, Shibata A, Jeggo PA, Löbrich M. 2017. DNA Double-Strand Break Resection Occurs during Non-homologous End Joining in G1 but Is Distinct from Resection during Homologous Recombination. *Mol Cell* **65**: 671-684.e675.

Blackford AN, Jackson SP. 2017. ATM, ATR, and DNA-PK: The Trinity at the Heart of the DNA Damage Response. *Mol Cell* **66**: 801-817.

Bredemeyer AL, Sharma GG, Huang CY, Helmink BA, Walker LM, Khor KC, Nuskey B, Sullivan KE, Pandita TK, Bassing CH et al. 2006. ATM stabilizes DNA double-strand-break complexes during V(D)J recombination. *Nature* **442**: 466-470.

Britton S, Chanut P, Delteil C, Barboule N, Frit P, Calsou P. 2020. ATM antagonizes NHEJ proteins assembly and DNA-ends synapsis at single-ended DNA double strand breaks. *Nucleic Acids Res* **48**: 9710-9723.

Bunting SF, Callén E, Wong N, Chen HT, Polato F, Gunn A, Bothmer A, Feldhahn N, Fernandez-Capetillo O, Cao L et al. 2010. 53BP1 inhibits homologous recombination in Brca1-deficient cells by blocking resection of DNA breaks. *Cell* **141**: 243-254.

Canela A, Sridharan S, Sciascia N, Tubbs A, Meltzer P, Sleckman BP, Nussenzweig A. 2016. DNA Breaks and End Resection Measured Genome-wide by End Sequencing. *Mol Cell* **63**: 898-911.

Chaplin AK, Hardwick SW, Liang S, Kefala Stavridi A, Hnizda A, Cooper LR, De Oliveira TM, Chirgadze DY, Blundell TL. 2021. Dimers of DNA-PK create a stage for DNA double-strand break repair. *Nat Struct Mol Biol* **28**: 13-19.

Chen BR, Wang Y, Tubbs A, Zong D, Fowler FC, Zolnerowich N, Wu W, Bennett A, Chen CC, Feng W et al. 2021a. LIN37-DREAM prevents DNA end resection and homologous recombination at DNA double-strand breaks in quiescent cells. *Elife* **10**.

Chen X, Xu X, Chen Y, Cheung JC, Wang H, Jiang J, de Val N, Fox T, Gellert M, Yang W. 2021b. Structure of an activated DNA-PK and its implications for NHEJ. *Mol Cell* **81**: 801-810.e803.

Clerici M, Mantiero D, Guerini I, Lucchini G, Longhese MP. 2008. The Yku70-Yku80 complex contributes to regulate double-strand break processing and checkpoint activation during the cell cycle. *EMBO Rep* **9**: 810-818.

Dev H, Chiang TW, Lescale C, de Krijger I, Martin AG, Pilger D, Coates J, Sczaniecka-Clift M, Wei W, Ostermaier M et al. 2018. Shieldin complex promotes DNA end-joining and counters homologous recombination in BRCA1-null cells. *Nat Cell Biol* **20**: 954-965.

Feng L, Chen J. 2012. The E3 ligase RNF8 regulates KU80 removal and NHEJ repair. *Nat Struct Mol Biol* **19**: 201-206.

Forment JV, Walker RV, Jackson SP. 2012. A high-throughput, flow cytometry-based method to quantify DNA-end resection in mammalian cells. *Cytometry A* **81**: 922-928.

Golub EI, Gupta RC, Haaf T, Wold MS, Radding CM. 1998. Interaction of human rad51 recombination protein with single-stranded DNA binding protein, RPA. *Nucleic Acids Res* **26**: 5388-5393.

Gottlieb TM, Jackson SP. 1993. The DNA-dependent protein kinase: requirement for DNA ends and association with Ku antigen. *Cell* **72**: 131-142.

Gravel S, Chapman JR, Magill C, Jackson SP. 2008. DNA helicases Sgs1 and BLM promote DNA double-strand break resection. *Genes Dev* **22**: 2767-2772.

Hammarsten O, Chu G. 1998. DNA-dependent protein kinase: DNA binding and activation in the absence of Ku. *Proc Natl Acad Sci U S A* **95**: 525-530.

Ishida N, Nakagawa T, Iemura SI, Yasui A, Shima H, Katoh Y, Nagasawa Y, Natsume T, Igarashi K, Nakayama K. 2017. Ubiquitylation of Ku80 by RNF126 Promotes Completion of Nonhomologous End Joining-Mediated DNA Repair. *Mol Cell Biol* **37**.

Ismail IH, Gagné JP, Genois MM, Strickfaden H, McDonald D, Xu Z, Poirier GG, Masson JY, Hendzel MJ. 2015. The RNF138 E3 ligase displaces Ku to promote DNA end resection and regulate DNA repair pathway choice. *Nat Cell Biol* **17**: 1446-1457.

Jackson SP, Bartek J. 2009. The DNA-damage response in human biology and disease. *Nature* **461**: 1071-1078.

Kent WJ, Sugnet CW, Furey TS, Roskin KM, Pringle TH, Zahler AM, Haussler D. 2002. The human genome browser at UCSC. *Genome Res* **12**: 996-1006.

Kent WJ, Zweig AS, Barber G, Hinrichs AS, Karolchik D. 2010. BigWig and BigBed: enabling browsing of large distributed datasets. *Bioinformatics* **26**: 2204-2207.

Koike-Yusa H, Li Y, Tan EP, Velasco-Herrera MeC, Yusa K. 2014. Genome-wide recessive genetic screening in mammalian cells with a lentiviral CRISPR-guide RNA library. *Nat Biotechnol* **32**: 267-273.

Langmead B, Trapnell C, Pop M, Salzberg SL. 2009. Ultrafast and memory-efficient alignment of short DNA sequences to the human genome. *Genome Biol* **10**: R25.

Lee SE, Moore JK, Holmes A, Umezu K, Kolodner RD, Haber JE. 1998. Saccharomyces Ku70, mre11/rad50 and RPA proteins regulate adaptation to G2/M arrest after DNA damage. *Cell* **94**: 399-409.

Li H, Handsaker B, Wysoker A, Fennell T, Ruan J, Homer N, Marth G, Abecasis G, Durbin R, Genome Project Data Processing S. 2009a. The Sequence Alignment/Map format and SAMtools. *Bioinformatics* **25**: 2078-2079.

Li H, Handsaker B, Wysoker A, Fennell T, Ruan J, Homer N, Marth G, Abecasis G, Durbin R, Subgroup GPDP. 2009b. The Sequence Alignment/Map format and SAMtools. *Bioinformatics* **25**: 2078-2079.

Ma Y, Pannicke U, Schwarz K, Lieber MR. 2002. Hairpin opening and overhang processing by an Artemis/DNA-dependent protein kinase complex in nonhomologous end joining and V(D)J recombination. *Cell* **108**: 781-794.

Ma Y, Schwarz K, Lieber MR. 2005. The Artemis:DNA-PKcs endonuclease cleaves DNA loops, flaps, and gaps. *DNA Repair (Amst)* **4**: 845-851.

Menon V, Povirk LF. 2016. End-processing nucleases and phosphodiesterases: An elite supporting cast for the non-homologous end joining pathway of DNA double-strand break repair. *DNA Repair (Amst)* **43**: 57-68.

Mimitou EP, Symington LS. 2008. Sae2, Exo1 and Sgs1 collaborate in DNA double-strand break processing. *Nature* **455**: 770-774.

Mirman Z, Lottersberger F, Takai H, Kibe T, Gong Y, Takai K, Bianchi A, Zimmermann M, Durocher D, de Lange T. 2018. 53BP1-RIF1-shieldin counteracts DSB resection through CST- and Polα-dependent fill-in. *Nature* **560**: 112-116.

Noordermeer SM, Adam S, Setiaputra D, Barazas M, Pettitt SJ, Ling AK, Olivieri M, Álvarez-Quilón A, Moatti N, Zimmermann M et al. 2018. The shieldin complex mediates 53BP1-dependent DNA repair. *Nature* **560**: 117-121.

Paiano J, Zolnerowich N, Wu W, Pavani R, Wang C, Li H, Zheng L, Shen B, Sleckman BP, Chen BR et al. 2021. Role of 53BP1 in end protection and DNA synthesis at DNA breaks. *Genes Dev* **35**: 1356-1367.

Paull TT, Gellert M. 1998. The 3' to 5' exonuclease activity of Mre 11 facilitates repair of DNA double-strand breaks. *Mol Cell* **1**: 969-979.

Postow L, Funabiki H. 2013. An SCF complex containing Fbxl12 mediates DNA damage-induced Ku80 ubiquitylation. *Cell Cycle* **12**: 587-595.

Postow L, Ghenoiu C, Woo EM, Krutchinsky AN, Chait BT, Funabiki H. 2008. Ku80 removal from DNA through double strand break-induced ubiquitylation. *J Cell Biol* **182**: 467-479.

Quinlan AR, Hall IM. 2010. BEDTools: a flexible suite of utilities for comparing genomic features. *Bioinformatics* **26**: 841-842.

San Filippo J, Sung P, Klein H. 2008. Mechanism of eukaryotic homologous recombination. *Annu Rev Biochem* **77**: 229-257.

Sartori AA, Lukas C, Coates J, Mistrik M, Fu S, Bartek J, Baer R, Lukas J, Jackson SP. 2007. Human CtIP promotes DNA end resection. *Nature* **450**: 509-514.

Scully R, Panday A, Elango R, Willis NA. 2019. DNA double-strand break repair-pathway choice in somatic mammalian cells. *Nat Rev Mol Cell Biol* **20**: 698-714.

Setiaputra D, Durocher D. 2019. Shieldin - the protector of DNA ends. *EMBO Rep* **20**.

Shao Z, Davis AJ, Fattah KR, So S, Sun J, Lee KJ, Harrison L, Yang J, Chen DJ. 2012. Persistently bound Ku at DNA ends attenuates DNA end resection and homologous recombination. *DNA Repair (Amst)* **11**: 310-316.

Shen W, Le S, Li Y, Hu F. 2016. SeqKit: A Cross-Platform and Ultrafast Toolkit for FASTA/Q File Manipulation. *PLoS One* **11**: e0163962.

Stiff T, O'Driscoll M, Rief N, Iwabuchi K, Löbrich M, Jeggo PA. 2004. ATM and DNA-PK function redundantly to phosphorylate H2AX after exposure to ionizing radiation. *Cancer Res* **64**: 2390-2396.

Sugiyama T, Kowalczykowski SC. 2002. Rad52 protein associates with replication protein A (RPA)-single-stranded DNA to accelerate Rad51-mediated displacement of RPA and presynaptic complex formation. *J Biol Chem* **277**: 31663-31672.

Symington LS, Gautier J. 2011. Double-strand break end resection and repair pathway choice. *Annu Rev Genet* **45**: 247-271.

Tkáč J, Xu G, Adhikary H, Young JTF, Gallo D, Escribano-Díaz C, Krietsch J, Orthwein A, Munro M, Sol W et al. 2016. HELB Is a Feedback Inhibitor of DNA End Resection. *Mol Cell* **61**: 405-418.

Trujillo KM, Yuan SS, Lee EY, Sung P. 1998. Nuclease activities in a complex of human recombination and DNA repair factors Rad50, Mre11, and p95. *J Biol Chem* **273**: 21447-21450.

Tubbs A, Sridharan S, van Wietmarschen N, Maman Y, Callen E, Stanlie A, Wu W, Wu X, Day A, Wong N et al. 2018. Dual Roles of Poly(dA:dT) Tracts in Replication Initiation and Fork Collapse. *Cell* **174**: 1127-1142.e1119.

Tzelepis K, Koike-Yusa H, De Braekeleer E, Li Y, Metzakopian E, Dovey OM, Mupo A, Grinkevich V, Li M, Mazan M et al. 2016. A CRISPR Dropout Screen Identifies Genetic Vulnerabilities and Therapeutic Targets in Acute Myeloid Leukemia. *Cell Rep* **17**: 1193-1205.

Wang H, Shi LZ, Wong CC, Han X, Hwang PY, Truong LN, Zhu Q, Shao Z, Chen DJ, Berns MW et al. 2013. The interaction of CtIP and Nbs1 connects CDK and ATM to regulate HR-mediated double-strand break repair. *PLoS Genet* **9**: e1003277.

Wang T, Wei JJ, Sabatini DM, Lander ES. 2014. Genetic screens in human cells using the CRISPR-Cas9 system. *Science* **343**: 80-84.

Weinfeld M, Soderlind KJ. 1991. 32P-postlabeling detection of radiation-induced DNA damage: identification and estimation of thymine glycols and phosphoglycolate termini. *Biochemistry* **30**: 1091-1097.

Wong N, John S, Nussenzweig A, Canela A. 2021. END-seq: An Unbiased, High-Resolution, and Genome-Wide Approach to Map DNA Double-Strand Breaks and Resection in Human Cells. *Methods Mol Biol* **2153**: 9-31.

Wright WD, Shah SS, Heyer WD. 2018. Homologous recombination and the repair of DNA double-strand breaks. *J Biol Chem* **293**: 10524-10535.

Yaneva M, Kowalewski T, Lieber MR. 1997. Interaction of DNA-dependent protein kinase with DNA and with Ku: biochemical and atomic-force microscopy studies. *EMBO J* **16**: 5098-5112.

Zahid S, Seif El Dahan M, Iehl F, Fernandez-Varela P, Le Du MH, Ropars V, Charbonnier JB. 2021. The Multifaceted Roles of Ku70/80. *Int J Mol Sci* **22**.

Zha S, Jiang W, Fujiwara Y, Patel H, Goff PH, Brush JW, Dubois RL, Alt FW. 2011. Ataxia telangiectasia-mutated protein and DNA-dependent protein kinase have complementary V(D)J recombination functions. *Proc Natl Acad Sci U S A* **108**: 2028-2033.

Zha S, Shao Z, Zhu Y. 2021. The plié by DNA-PK: dancing on DNA. *Mol Cell* **81**: 644-646.

Zhou Y, Paull TT. 2013. DNA-dependent protein kinase regulates DNA end resection in concert with Mre11-Rad50-Nbs1 (MRN) and ataxia telangiectasia-mutated (ATM). *J Biol Chem* **288**: 37112-37125.

Zhu Z, Chung WH, Shim EY, Lee SE, Ira G. 2008. Sgs1 helicase and two nucleases Dna2 and Exo1 resect DNA double-strand break ends. *Cell* **134**: 981-994.